

# Evaluation of multiaxial stress-strain models and fatigue life prediction methods under proportional loading

Marco Antonio Meggiolaro, Jaime Tupiassú Pinho de Castro  
*Department of Mechanical Engineering, Pontifical Catholic University of Rio de Janeiro, Rio de Janeiro/RJ – Brazil*

Antonio Carlos de Oliveira Miranda  
*Tecgraf, Pontifical Catholic University of Rio de Janeiro, Rio de Janeiro/RJ – Brazil*

## Abstract

Multiaxial fatigue damage occurs when the principal stress directions vary during the loading induced by several independent forces, such as out-of-phase bending and torsion. Uniaxial damage models cannot be reliably applied in this case. Besides the need for multiaxial damage models, another key issue to reliably model such problems is how to calculate the elastic-plastic stresses from the multiaxial strains. Hooke's law cannot be used to correlate stresses and strains for short lives due to plasticity effects. Ramberg-Osgood cannot be used either to directly correlate principal stresses and strains under multiaxial loading, because this model has been developed for the uniaxial case. The purpose of this work is to critically review and compare the main fatigue crack initiation models under multiaxial loading. The studied models include stress-based ones such as Sines, Findley and Dang Van, and strain-based ones such as the  $\gamma N$  curve, Brown-Miller, Fatemi-Socie and Smith-Watson-Topper models. Modified formulations of the strain-based models are presented to incorporate Findley's idea of using critical planes that maximize damage. To incorporate plasticity effects, four models are studied and compared to correlate stresses and strains under proportional loading: the method of the highest  $K_t$ , the constant ratio model, Hoffmann-Seeger's and Dowling's models.

Keywords: multiaxial fatigue, crack initiation, life prediction models, stress-strain models.

## 1 Introduction

Real loads can induce combined bending, torsional, axial and shear stresses, which can generate bi- or tri-axial variable stress/strain histories at the critical point (in general a notch root), causing the so-called multiaxial fatigue problems. The load history is said to be proportional when it generates stresses with principal axes which maintain a fixed orientation, while non-proportional loading is associated with principal directions which change in time during the loading history.

24 For periodic loads with same frequency, one can also define the concept of in-phase and out-of-phase  
 25 loading. In-phase loading always leads to proportional histories, however the opposite is not true: e.g.,  
 26 the stresses  $\sigma_x = \sigma_I$  and  $\sigma_y = \sigma_{II}$  induced on a plate by perpendicular ( $\perp$ ) forces  $F_x$  and  $F_y$  are always  
 27 proportional, because the principal axes maintain a fixed direction even if  $F_x$  and  $F_y$  are out-of-phase.

28 On the other hand, out-of-phase axial and torsional stresses always generate non-proportional (NP)  
 29 loading [1]. The non-proportionality factor  $F_{np}$  of the applied loads can be obtained from the shape of the  
 30 ellipse that encloses the history of normal and shear strains induced by them,  $\varepsilon$  and  $\gamma$ . Considering  
 31  $a$  and  $b$  ( $b \leq a$ ) as the semi-axes of the ellipsis which encloses the strain path in the Mises diagram  
 32  $\varepsilon \times \gamma/\sqrt{3}$ , then the non-proportionality factor  $F_{np}$  is defined as  $b/a$  ( $0 \leq F_{np} \leq 1$ ), see Fig. 1. A  
 33 further discussion on enclosing ellipses, and hyper-ellipsoids, can be found in [2].

34 All proportional loadings have shear strains  $\gamma$  proportional to the normal strains  $\varepsilon$ , with  $F_{np} = 0$  and  
 35 a straight-line trajectory in the  $\varepsilon \times \gamma/\sqrt{3}$  diagram. Any loading history with  $F_{np} > 0$  is NP. Note e.g.  
 36 that the loading ( $\sigma_a \sin \omega t + \tau_a \cos \omega t$ ) with  $\tau_a = \sigma_a \sqrt{3}/2(1 + \nu)$ , caused by a traction and a properly  
 37 scaled torsion  $90^\circ$  out of phase, has  $F_{np} = 1$ , therefore the maximum possible non-proportionality.

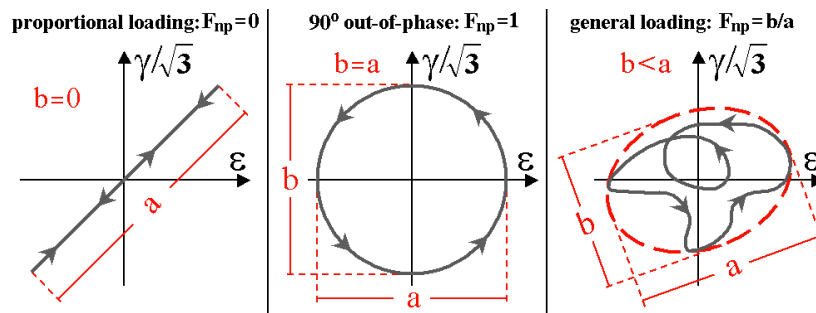


Figure 1: Diagram  $\varepsilon \times \gamma/\sqrt{3}$ , and associated non-proportionality factors (Socie and Marquis, 1999).

38 Predictions with NP histories can be very complex, because they involve at least three potential  
 39 problems:

- 40 1. NP hardening: the cyclic hardening coefficient  $H_c$  and the ratio  $\Delta\sigma/\Delta\varepsilon$  of a few materials increase  
 41 under NP loading, which significantly decreases the fatigue life of parts subject to a constant  
 42  $\Delta\varepsilon$ ;
- 43 2. Damage calculation: the SN and  $\varepsilon N$  curves, measured under proportional loading, cannot be  
 44 directly used when principal directions vary, because in this case the crack propagation plane in  
 45 general does not match the one from the tests; and
- 46 3. Cycle counting: the traditional rain-flow counting techniques cannot be applied to variable ampli-  
 47 tude NP loading, because the peaks and valleys of  $\varepsilon$  in general do not match with the ones of  
 48  $\gamma$ , becoming impossible to decide *a priori* which points should be accounted for.

49 The first two problems will be addressed in this work. A NP hardening model will be presented,  
 50 to allow for the correct calculation of the equivalent stresses, and multiaxial models based on stress

51 or strain measurements will be used to calculate the damage generated both by proportional and NP  
52 loadings.

53 A few classical models that correlate stresses or strains with multiaxial fatigue life are studied below.  
54 Stress-based models (which can be applied for long life predictions) proposed by Sines, Findley and  
55 Dang Van are presented, as well as strain-based models proposed by Brown-Miller, Fatemi-Socie and  
56 Smith-Watson-Topper (SWT), which must be used for short lives.

57 One problem with the application of the Fatemi-Socie or SWT models is the need to calculate the  
58 elastic-plastic stresses from the multiaxial strains, because Ramberg-Osgood is only valid for uniaxial  
59 stresses. Another challenge in multiaxial fatigue life calculations is the modeling of the notch effect.  
60 The elastic stress concentration factor  $K_\sigma$  and strain concentration factor  $K_\epsilon$  are the same for uniaxial  
61 loading, but in general in the multiaxial case  $K_\sigma$  is different from  $K_\epsilon$  even under elastic stresses.

62 Therefore, even in the elastic case, it is not trivial to study the notch effect under multiaxial  
63 loading. The problem is worse in the elastic-plastic case, where even uniaxial loadings can generate  
64 NP multiaxial stress and strain histories, due to the tri-axial stress state at the notch root and  
65 to the difference between the elastic and plastic Poisson coefficients. Typically, metallic alloys have  
66  $1/4 \leq \nu_{el} \leq 1/3$  and  $\nu_{pl} = 0.5$ . In the following sections the multiaxial stress-strain models are  
67 presented and compared, including notch effects.

## 68 2 Non-proportional loading

69 A few materials under NP cyclic loading can harden much more than it would be predicted from  
70 the traditional cyclic  $\sigma\epsilon$  curve. This phenomenon, called NP hardening, depends on the load history  
71 (through the NP factor  $F_{np}$ ) and on the material (through a constant  $\alpha_{np}$  of NP hardening, where  
72  $0 \leq \alpha_{np} \leq 1$ ). The NP hardening can be modeled in general using the same Ramberg-Osgood plastic  
73 exponent  $h_c$  from the uniaxial cyclic  $\sigma\text{-}\epsilon$  curve, and using a new coefficient  $H_{cnp} = H_c \cdot (1 + \alpha_{np} \cdot F_{np})$ ,  
74 where  $H_c$  is the uniaxial Ramberg-Osgood plastic coefficient, see Fig. 2. Note that the NP hardening  
75 can multiply the uniaxial strain hardening coefficient  $H_c$  by a value as high as 2.

76 The largest NP hardening occurs when  $F_{np} = 1$ , e.g. under a properly scaled traction-torsion loading  
77  $90^\circ$  out of phase which generates a circle in the  $\epsilon \times \gamma/\sqrt{3}$  Mises diagram.

78 Typically, the NP hardening effect is high in austenitic stainless steels at room temperature ( $\alpha_{np} \cong 1$   
79 in the stainless steel 316), medium in carbon steels ( $\alpha_{np} \cong 0.3$  in the 1045 steel) and low in aluminum  
80 alloys ( $\alpha_{np} \cong 0$  for Al 7075). Note that proportional histories do not lead to NP hardening.

81 The NP hardening happens in materials with low fault stacking energy (which in austenitic stainless  
82 steels is only  $23\text{mJ/m}^2$ ) and well spaced dislocations, where the slip bands generated by proportional  
83 loading are always planar. In these materials, the NP loads activate crossed slip bands in several  
84 directions (due to the rotation of the maximum shear planes), therefore increasing the hardening  
85 effect ( $\alpha_{np} \gg 0$ ) with respect to the proportional loadings. But in materials with high fault stacking  
86 energy (such as aluminum alloys, with a typical value of  $250\text{mJ/m}^2$ ) and with close dislocations,  
87 the crossed slip bands already happen naturally even under proportional loading, therefore the NP  
88 histories do not cause any significant difference in hardening ( $\alpha_{np} \cong 0$ ).

89 But the Coffin-Manson or the Morrow crack initiation equations cannot account for the influence of

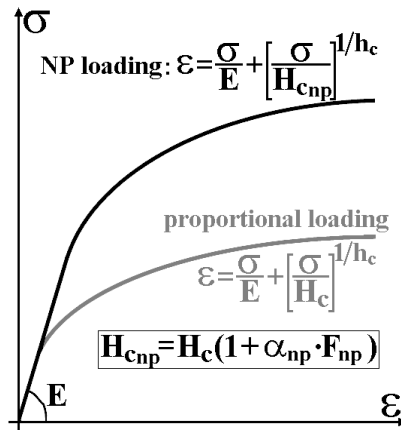


Figure 2: Effect of cyclic NP loadings on the NP hardening.

90 NP hardening. This implies that the use of traditional  $\varepsilon N$  equations, which were developed to model  
 91 uniaxial fatigue problems, can be non-conservative when the loading histories are NP.

92 However, it must be noted that the NP hardening reduces fatigue life only in strain-controlled  
 93 problems (such as in  $\varepsilon N$  specimen tests or very sharp notches, e.g.), because the stresses  $\Delta\sigma$  caused  
 94 by a given  $\Delta\varepsilon$  are higher than in the proportional case. But in stress-controlled problems (the most  
 95 common case in practice), the  $\Delta\varepsilon$  generated by a given  $\Delta\sigma$  is lower under NP loading, therefore the  
 96 fatigue life is higher than in the proportional case (the uniaxial  $\varepsilon N$  equations can lead to conservative  
 97 predictions in this case). In the following sections, the multiaxial models to predict NP damage are  
 98 studied.

### 99 3 Stress-based multiaxial fatigue damage models

100 It is well known that Tresca or Mises equivalent stresses must be used to predict crack initiation lives,  
 101 which depend on the cyclic movement of dislocations. However, crack initiation can and should be  
 102 divided into:

- 103 • formation of microcracks, which is almost insensitive to mean stresses and hydrostatic pressure  
 104 in metals, because it only depends on dislocation movement; followed by
- 105 • propagation of the dominant microcrack, which also depends on the crack face opening and the  
 106 friction between the faces, becoming increasingly sensitive to the applied mean stress  $\sigma_m$  as the  
 107 microcrack grows.

108 Microcracks are cracks with sizes up to the order of the metal grain sizes. Their modeling using  
 109 classical fracture mechanics is questionable, as opposed to long cracks (typically larger than 1 or 2mm),  
 110 which have crack propagation rates controlled by  $\Delta K$ .

111 However, SN and  $\epsilon$ N tests bring test specimens (TS) to fracture, or to the generation of a small,  
 112 finite crack, therefore they include both microcrack initiation and propagation phases. Thus, since the  
 113 shear stress  $\Delta\tau$  controls the initiation of a microcrack, while the normal stress  $\sigma_{\perp}$  perpendicular to  
 114 its plane (or the hydrostatic stress  $\sigma_h$ , invariant defined as the mean of the normal stresses) controls  
 115 its opening, both are important to predict the fatigue lives of SN and  $\epsilon$ N specimens.

116 In fact, a component under uniaxial traction  $\sigma_x = \sigma$  and another under torsion  $\tau_{xy} = \sigma/2$  work under  
 117 the same Tresca equivalent stress, but the microcracks on the plane of  $\tau_{max}$  in the first component  
 118 are subject to a normal stress  $\sigma_{\perp}$  perpendicular to that plane that tends to keep their mouth open,  
 119 exposing the crack tips and decreasing the crack face friction, see Fig. 3. Therefore, the fatigue damage  
 120 generated by  $\Delta\sigma$  can be greater than the one caused by the pure torsion  $\Delta\tau = \Delta\sigma/2$ .

121 The Mises equivalent stress is able to, at least in part, consider such effect, because the component  
 122 under torsion would have  $\sigma_{Mises} = \tau_{xy}\sqrt{3} = 0.866 \cdot \sigma_x < \sigma$ , however  $\sigma_{Mises}$  is insensitive to the  
 123 hydrostatic stress  $\sigma_h$ . The Mises shear strain  $\tau_{Mises}$ , which acts on the octahedric planes, does not  
 124 consider as well the effects of  $\sigma_h$ , relating with  $\sigma_{Mises}$  through:

$$\begin{aligned} \sigma_{Mises} &= \frac{3}{\sqrt{2}}\tau_{Mises} = \frac{1}{\sqrt{2}}\sqrt{(\sigma_1 - \sigma_2)^2 + (\sigma_1 - \sigma_3)^2 + (\sigma_2 - \sigma_3)^2} = \\ &= \frac{1}{\sqrt{2}}\sqrt{(\sigma_x - \sigma_y)^2 + (\sigma_y - \sigma_z)^2 + (\sigma_x - \sigma_z)^2 + 6(\tau_{xy}^2 + \tau_{yz}^2 + \tau_{xz}^2)} \end{aligned} \tag{1}$$

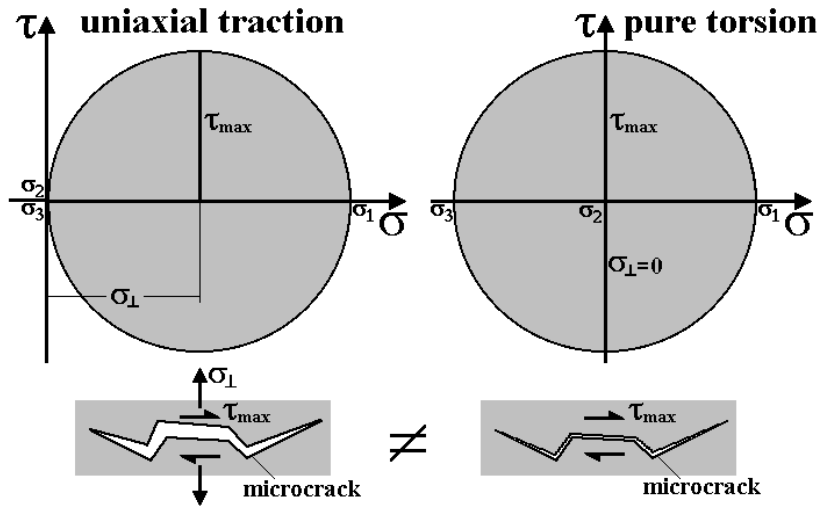


Figure 3: Mohr circles showing why under the same  $\Delta\sigma_{Tresca}$  equivalent loading the component under pure torsion can have a higher fatigue life than the one under pure traction.

125 Sines [3] has proposed a fatigue failure criterion under proportional multiaxial stresses, based on  
 126  $\Delta\tau_{Mises}$  and on  $\sigma_{hm} = (\sigma_{xm} + \sigma_{ym} + \sigma_{zm})/3$ , the hydrostatic component of the mean stresses (insen-  
 127 sitive to the shear stresses):

$$\frac{\Delta\tau_{Mises}}{2} + \alpha_S \cdot (3 \cdot \sigma_{hm}) = \beta_S \quad (2)$$

128 where  $\alpha_S$  and  $\beta_S$  are adjustable constants for each material, and

$$\Delta\tau_{Mises} = \frac{1}{3} \sqrt{(\Delta\sigma_1 - \Delta\sigma_2)^2 + (\Delta\sigma_1 - \Delta\sigma_3)^2 + (\Delta\sigma_2 - \Delta\sigma_3)^2} \quad (3)$$

129 In this way, according to the Sines criterion, a component will have infinite fatigue life under  
 130 proportional loading if

$$\Delta\tau_{Mises}/2 + \alpha_S \cdot (3 \cdot \sigma_{hm}) < \beta_S \quad (4)$$

131 On the other hand, the Findley [4] criterion, which is also applicable to NP multiaxial loadings,  
 132 assumes that the crack initiates at the critical plane of the critical point. This idea is interesting,  
 133 because it is on this plane that the damage caused by the combination  $\Delta\tau/2 + \alpha_F \cdot \sigma_{\perp}$  is maximum,  
 134 where  $\Delta\tau/2$  is the shear stress amplitude on that plane and  $\sigma_{\perp}$  is the normal stress perpendicular to  
 135 it. Thus, according to Findley the fatigue failure criterion at the critical plane of the critical point is

$$\left( \frac{\Delta\tau}{2} + \alpha_F \cdot \sigma_{\perp} \right)_{\max} = \beta_F \quad (5)$$

136 where  $\alpha_F$  and  $\beta_F$  are constants which must be fitted by measurements in at least two types of fatigue  
 137 tests, e.g., under rotating bending and under pure torsion, or in push-pull tests under two different R  
 138 ratios.

139 The critical plane can vary at each i-th event of the NP loads, even when the critical point remains  
 140 the same, but Findley predicts fatigue failure based on the plane where the sum of the damages  
 141 associated with  $[\Delta\tau_i(\theta)/2 + \alpha_F \cdot \sigma_{\perp_i}(\theta)]$  is maximum, where  $\theta$  is the angle of such plane with respect  
 142 to a reference direction.

143 Under pure torsion, Eq. (5) can be written as

$$\sqrt{1 + \alpha_F^2} \cdot \frac{\Delta\tau}{2} = \beta_F \quad (6)$$

144 And under cyclic uniaxial traction with alternate component  $\sigma_a$  and maximum component  $\sigma_{max}$ ,  
 145 it can be shown that Findley's criterion can be written as

$$0.5\sigma_a \left[ \sqrt{1 + \left( \frac{2\alpha_F}{1-R} \right)^2} + \frac{2\alpha_F}{1-R} \right] = \beta_F \quad (7)$$

146 where  $R = \sigma_{min}/\sigma_{max}$  is the stress ratio, which quantifies the mean stress effects.

147 Therefore, from Findley it is possible to estimate the fatigue limit  $S_L(R)$  under any ratio  $R$  from  
 148  $\alpha_F$  and the fatigue limit  $S_L$  (obtained under zero mean loads, i.e., with  $R = -1$ , see Fig. 4) through

$$\frac{S_L(R)}{S_L} = \frac{\sigma_a(R)}{\sigma_a} = \frac{\sqrt{1 + \alpha_F^2} + \alpha_F}{\sqrt{1 + \left(\frac{2\alpha_F}{1-R}\right)^2} + \frac{2\alpha_F}{1-R}} \quad (8)$$

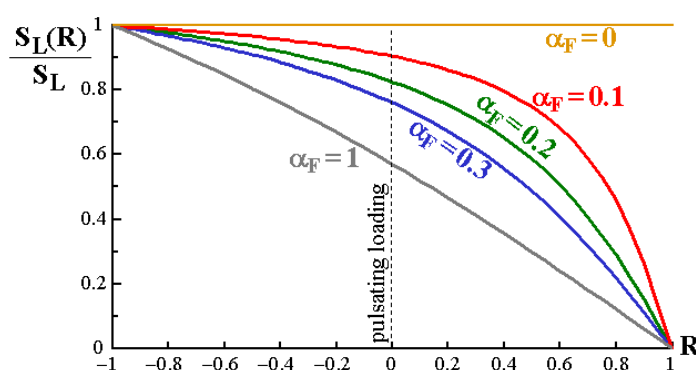


Figure 4: Fatigue limit  $S_L(R)$  as a function of  $R$ , according to Findley.

149 From the principle that the damage associated with the initiation of fatigue microcracks cannot  
 150 be detected from macroscopic measurements, Dang Van [5] proposed a model that considers the  
 151 variable micro stresses that act inside a characteristic volume element (VE) of the material, where  
 152 the macroscopic stresses and strains are supposedly constant. The VE is the unit used in structural  
 153 analysis to represent the material properties, such as its Young modulus and its several strengths. Thus  
 154 the VE must be small compared to the component's dimensions, but large compared to the parameter  
 155 that characterizes the intrinsic anisotropy of the material. For instance, a VE of only  $1\text{mm}^3$  is sufficient  
 156 for most structural metal alloys, which have a grain size  $g$  typically between 10 and  $100\mu\text{m}$  (the grain  
 157 itself, being a monocrystal, is intrinsically anisotropic).

158 Inside a VE, the local micro stresses  $[\sigma_{ij}]_\mu = \sigma_\mu$  and strains  $[\varepsilon_{ij}]_\mu = \varepsilon_\mu$  acting between grains, or  
 159 between them and small imperfections such as inclusions, e.g., can significantly differ from the macro  
 160 stresses  $[\sigma_{ij}]_M = \sigma_M$  and strains  $[\varepsilon_{ij}]_M = \varepsilon_M$ , assumed constant in the macroscopic analysis normally  
 161 used in mechanical design. Therefore, these micro quantities can significantly influence crack initiation.  
 162 Note that if the term “microscopic” is reserved to the scale associated with interatomic stresses, domain  
 163 of solid state physics, then its is recommended to use the term “mesoscopic” to describe the intra or  
 164 intergranular stresses. Thus, the macroscopic stresses reflect the average of the mesoscopic stresses in  
 165 a VE:  $\sigma_M = \int \sigma_\mu dV/V$ , where  $V$  is the volume of the VE. Similarly,  $\varepsilon_M = \int \varepsilon_\mu dV/V$ .

166 In other words, the macroscopic stresses and strains are assumed constant at the characteristic  
 167 volume element VE of the material, however the mesoscopic intergranular stresses can vary a lot,  
 168 influencing crack initiation.

169 Since the microcracks initiate at persistent slip bands, Dang Van assumed that fatigue damage was  
 170 caused by the mesoscopic shear strain history  $\tau_\mu(t)$  and influenced by the mesoscopic hydrostatic stress  
 171 history  $\sigma_{\mu h}(t)$ . The simplest failure criterion involving these components is the linear combination  
 172 given by:

$$\tau_\mu(t) + \alpha_{DV} \cdot \sigma_{\mu h}(t) = \beta_{DV} \quad (9)$$

173 Note that the Sines, Findley and Dang Van criteria can be included in the general class of Mohr  
 174 models against material failure, which use combinations of the shear stress  $\tau$  that acts on a certain  
 175 plane with the normal or hydrostatic stresses  $\sigma$  on this plane:

$$\tau + \alpha \cdot \sigma = \beta \quad (10)$$

176 The Sines criterion uses the Mises or octahedric plane and the hydrostatic stresses, therefore  $\tau \equiv$   
 177  $\Delta\tau_{Mises}/2$ ,  $\sigma \equiv 3 \cdot \sigma_{hm}$ ,  $\alpha \equiv \alpha_S$ ,  $\beta \equiv \beta_S$ ; Findley uses the shear stress on the critical plane and the  
 178 normal stress perpendicular to it, thus  $\tau \equiv \Delta\tau/2$ ,  $\sigma \equiv \sigma_\perp$ ,  $\alpha \equiv \alpha_F$ ,  $\beta \equiv \beta_F$ ; and Dang Van can be  
 179 obtained from  $\tau \equiv \tau_\mu(t)$ ,  $\sigma \equiv \sigma_{\mu h}(t)$ ,  $\alpha \equiv \alpha_{DV}$ ,  $\beta \equiv \beta_{DV}$ . Other similar criteria can be found in [1]  
 180 and [6].

181 Finally, it is important to remember that the SN and  $\varepsilon$ N tests involve both microcrack initiation  
 182 (sensitive to  $\tau$ ) and propagation (more sensitive to  $\sigma$ ) phases, and therefore fatigue damage can be  
 183 more influenced by  $\tau$  or  $\sigma$ , depending on the percentage of the life spent at each phase. Therefore,  
 184 materials with large values of  $\alpha$  are more sensitive to  $\sigma$  (normal stresses are more important to them),  
 185 probably spending more cycles to propagate than to initiate the microcrack.

#### 186 4 Strain-based multiaxial fatigue damage models

187 The three multiaxial failure criteria presented above are based on macroscopic stresses that are sup-  
 188 posedly elastic, therefore they are only applicable when  $\sigma_{Mises}$  is much smaller than the cyclic yielding  
 189 strength  $S_{yc}$ . Thus, as in the case of the SN method, they should only be used to predict long fatigue  
 190 lives. Otherwise, it is imperative to use fatigue damage criteria based on applied strains instead of  
 191 stresses [1], using the principles studied in the so-called  $\varepsilon$ N method.

192 One of the simplest models is the one based on the  $\gamma$ N curve, similar to Coffin-Manson's equation,  
 193 which uses the largest shear strain range  $\Delta\gamma_{max}$  acting on the specimen ( $\gamma_{ij}$  ( $2\varepsilon_{ij}$ ,  $i \neq j$ )) to predict  
 194 fatigue life

$$\frac{\Delta\gamma_{max}}{2} = \frac{\tau_c}{G} (2N)^{b_\gamma} + \gamma_c (2N)^{c_\gamma} \quad (11)$$

195 where  $\tau_c$ ,  $b_\gamma$ ,  $\gamma_c$  and  $c_\gamma$  are parameters similar to the ones used in Coffin-Manson's equation. In this  
 196 way, since the shear modulus  $G = E/[2(1 + \nu)]$ ,  $\nu$  being Poisson's coefficient, if no experimental data

197 is available, then the  $\gamma N$  curve can be estimated assuming  $\tau_c \cong \sigma_c/\sqrt{3}$ ,  $b_\gamma \cong b$ ,  $\gamma_c \cong \varepsilon_c\sqrt{3}$  and  $c_\gamma \cong c$ ,  
 198 resulting in

$$\frac{\Delta\gamma_{\max}}{2} \cong \frac{\sigma_c}{E} \frac{2(1+\nu)}{\sqrt{3}} (2N)^b + \varepsilon_c \sqrt{3} (2N)^c \quad (12)$$

199 The  $\gamma N$  curve is only recommended to model fatigue damage in materials that are more sensitive  
 200 to shear strains (which have small  $\alpha$  in the Mohr models), and if the mean loads are zero. It would be  
 201 expected that such materials would have a shorter torsional fatigue life than similar materials more  
 202 sensitive to normal stresses.

203 The Brown-Miller [7] model can consider the mean stress effects, combining the maximum range of  
 204 the shear strain  $\Delta\gamma_{\max}$  to the range of normal strain  $\Delta\varepsilon_\perp$  (through the term  $\Delta\gamma_{\max}/2 + \alpha_{BM} \cdot \Delta\varepsilon_\perp$ )  
 205 and the mean normal stress  $\sigma_{\perp m}$  perpendicular to the plane of maximum shear strain, to obtain the  
 206 fatigue life  $N$ :

$$\frac{\Delta\gamma_{\max}}{2} + \alpha_{BM} \cdot \Delta\varepsilon_\perp = \beta_1 \frac{\sigma_c - 2\sigma_{\perp m}}{E} (2N)^b + \beta_2 \varepsilon_c (2N)^c \quad (13)$$

207 where  $\alpha_{BM}$  is a fitting parameter ( $\alpha_{BM} \cong 0.3$  for ductile metals in lives near the fatigue limit),  
 208  $\beta_1 = (1 + \nu + (1 - \nu) \cdot \alpha_{BM})$ , and  $\beta_2 = 1.5 + 0.5 \cdot \alpha_{BM}$ .

209 This equation was adapted from Morrow to fit uniaxial traction test data, where the mean stress  
 210  $\sigma_m$  is equal to  $2\sigma_{\perp m}$  (because  $\sigma_{\perp m}$  acts perpendicularly to the plane of  $\gamma_{\max}$ , therefore it is worth  
 211 half of  $\sigma_m$ ).

212 The values of  $\beta_1$  and  $\beta_2$  are obtained assuming uniaxial traction, see Fig. 5:

$$\left. \begin{array}{l} \Delta\gamma_{\max} = (1 + \nu)\Delta\varepsilon \\ \Delta\varepsilon_\perp = (1 - \nu)\Delta\varepsilon/2 \end{array} \right\} \Rightarrow \frac{\Delta\gamma_{\max}}{2} + \alpha_{BM}\Delta\varepsilon_\perp = \frac{\Delta\varepsilon}{2} [(1 + \nu) + \alpha_{BM}(1 - \nu)] \quad (14)$$

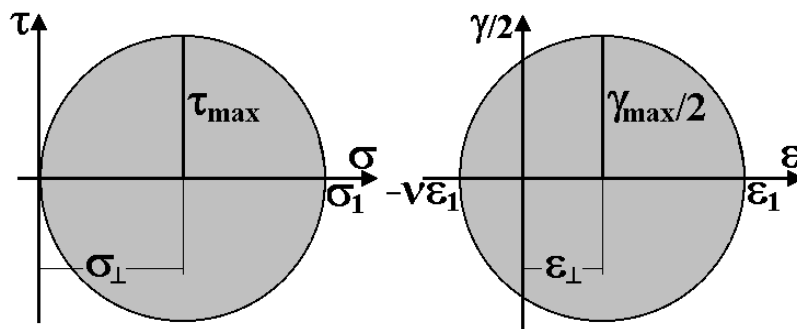


Figure 5: Mohr circles for stresses and strains under uniaxial traction.

From Eq. (14), the coefficients  $\beta_1 = (1 + \nu) + (1 - \nu) \cdot \alpha_{BM}$  and  $\beta_2 = 1.5 + 0.5 \cdot \alpha_{BM}$  are obtained, because  $\nu = 0.5$  for plastic strains, which preserve volume. The original Brown-Miller model assumes that the elastic strains have  $\nu = 0.3$ , therefore  $\beta_1 \cong (1 + 0.3) + (1 - 0.3) \cdot \alpha_{BM} = 1.3 + 0.7 \cdot \alpha_{BM}$ .

The Brown-Miller model is frequently used in multiaxial fatigue, even though it is not reasonable to assume that  $\Delta\varepsilon_\perp$  can control the opening and closure of microcracks, because the range  $\Delta\varepsilon$  does not include information about maximum stresses or strains. E.g., two microcracks with the same  $\Delta\gamma_{max}$  and  $\Delta\varepsilon_\perp$  can have very different fatigue lives if one is opened (under traction) and the other closed (under compression) due to the mean load effect. The use of  $\sigma_{\perp m}$  compensates in part for this model flaw, however the mean stress effect is only considered in the elastic part.

Fatemi and Socie [8] suggested replacing  $\Delta\varepsilon_\perp$  by the maximum normal stress  $\sigma_{\perp max}$  perpendicular to the plane of maximum shear strain, applying it to the  $\gamma N$  curve:

$$\frac{\Delta\gamma_{max}}{2} \left( 1 + \alpha_{FS} \frac{\sigma_{\perp max}}{S_{yc}} \right) = \frac{\tau_c}{G} (2N)^{b_\gamma} + \gamma_c (2N)^{c_\gamma} \quad (15)$$

Note that the value of  $\alpha_{BM}$  and  $\alpha_{FS}$  indicates whether the material is more sensitive to  $\tau$  ( $\alpha_{BM}$  or  $\alpha_{FS} \ll 1$ ) or to  $\sigma$  ( $\alpha_{BM}$  or  $\alpha_{FS} \gg 1$ ).

If the propagation phase of the microcracks (more sensitive to  $\sigma$ ) is dominant over initiation, the Smith-Watson-Topper (SWT) multiaxial model can be used [9]:

$$\frac{\Delta\varepsilon_1}{2} \cdot \sigma_{\perp 1 max} = \frac{\sigma_c^2}{E} (2N)^{2b} + \sigma_c \varepsilon_c (2N)^{b+c} \quad (16)$$

where  $\Delta\varepsilon_1$  is the range of the maximum principal strain and  $\sigma_{(1max)}$  is the stress peak in the direction perpendicular to  $\varepsilon_1$ .

Figure 6 summarizes the parameters used in the above strain-based models. In addition, there are several other models based on the plastic energy dissipated by the hysteresis loops, and other combining energy with critical planes, see [1].

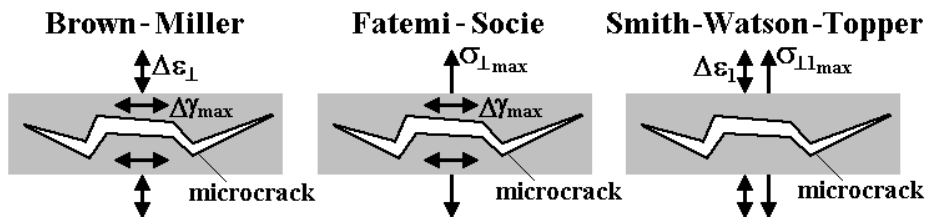


Figure 6: Parameters which affect the strain-based multiaxial models.

It is important to note that the plane of maximum shear strain amplitude  $\Delta\gamma_{max}/2$  (used in Brown-Miller's and Fatemi-Socie's models) is in general different from the planes that would maximize the respective damage parameters ( $\Delta\gamma/2 + \alpha_{BM}(\Delta\varepsilon_\perp)$  for Brown-Miller, and  $\Delta\gamma((1 + \alpha_{FS}(\sigma_{\perp max}/S_{yc}))/2$

236 for Fatemi-Socie). But if these are the parameters that cause damage, it is reasonable to argue that  
 237 fatigue life should be calculated on the critical plane that maximizes them (in a similar way as done  
 238 in Findley's model), and not on the plane of  $\Delta\gamma_{max}$ . In this way, it is a good idea to modify the  
 239 Brown-Miller and Fatemi-Socie models introducing a subtle but important change:

$$\frac{\Delta\gamma_{max}}{2} + \alpha_{BM} \cdot \Delta\varepsilon_{\perp} \Rightarrow \left( \frac{\Delta\gamma}{2} + \alpha_{BM} \cdot \Delta\varepsilon_{\perp} \right)_{max} \quad (17)$$

240

$$\frac{\Delta\gamma_{max}}{2} \left( 1 + \alpha_{FS} \frac{\sigma_{\perp max}}{S_{yc}} \right) \Rightarrow \left( \frac{\Delta\gamma}{2} + \alpha_{FS} \frac{\Delta\gamma}{2} \frac{\sigma_{\perp\gamma}}{S_{yc}} \right)_{max} \quad (18)$$

241 The use of critical planes that maximize the damage parameters in each model has the advantage of  
 242 predicting not only the fatigue life but also the dominant planes where the crack will initiate. However,  
 243 these calculations are not simple and require the use of sophisticated numerical methods.

244 This idea can also be applied to the SWT model, calculating the critical plane where the product  
 245 between the normal strain range  $\Delta\varepsilon_{\perp}$  and the normal stress peak  $\sigma_{\perp max}$  is maximized, adopting the  
 246 modification

$$\frac{\Delta\varepsilon_{\perp}}{2} \cdot \sigma_{\perp max} \Rightarrow \left( \frac{\Delta\varepsilon_{\perp}}{2} \cdot \sigma_{\perp max} \right)_{max} \quad (19)$$

247 A great advantage of the Fatemi-Socie (or SWT) model is to be able to consider the effect of NP  
 248 hardening from the peak of normal stress  $\sigma_{\perp max}$  (or  $\sigma_{\perp 1max}$ ). In stainless steels, e.g., a NP history  
 249 leads to a much higher damage than a proportional one with the same  $\Delta\gamma_{max}$  and  $\Delta\varepsilon_{\perp}$ , because the  
 250 NP hardening increases the value of  $\sigma_{\perp max}$  (or  $\sigma_{\perp 1max}$ ). Note that Brown-Miller would wrongfully  
 251 predict the same damage in both histories (because  $\Delta\gamma_{max}$  and  $\Delta\varepsilon_{\perp}$  would be the same), and only  
 252 the Fatemi-Socie and SWT models would be able to correctly account for the greater damage of the  
 253 NP loading (assuming that  $H_{cnp}$  would be used to obtain  $\sigma_{\perp max}$  and  $\sigma_{\perp 1max}$ ).

## 254 5 Multiaxial stress-strain relations

255 Hooke's law cannot be used to correlate stresses and strains for short multiaxial fatigue life predictions,  
 256 due to plasticity effects. The hookean stresses and strains,  $\tilde{\sigma}$  and  $\tilde{\varepsilon}$ , defined as the values of  $\sigma$  and  $\varepsilon$   
 257 obtained assuming that the material would be linear elastic (using Hooke's law and, at the notches,  
 258 considering elastic  $K_{\sigma}$  and  $K_{\varepsilon}$ ), can only be applied for long life predictions.

259 In addition, Ramberg-Osgood cannot be used either to directly correlate principal stresses and  
 260 strains  $\sigma_i$  and  $\varepsilon_i$  ( $i = 1, 2, 3$ ) of a multiaxial history, because this model has been developed for the  
 261 uniaxial case.

262 However, if the elastic nominal stress range  $\Delta\sigma_n$  is caused by in-phase loading, then it is trivial to  
 263 calculate the elastic-plastic stresses and strains at the notch root using the "highest  $K_t$  method". In this  
 264 approximate method, the equivalent nominal stress range  $\Delta\sigma_n$  calculated from Tresca or Mises is used  
 265 to obtain  $\Delta\sigma$  and  $\Delta\varepsilon$  at the notch root using Ramberg-Osgood and (for safety, because the method  
 266 is conservative) the highest  $K_t$  in Neuber's rule. Remember that the multiaxial loadings can result, at

the same notch root, in different values of  $K_t$  for traction, bending, torsion and shear loadings, but only the maximum one is used. To generate more accurate predictions for notches under combined stresses, it is recommended to use multiaxial  $\sigma$ - $\varepsilon$  relations.

Several models have been proposed to correlate  $\sigma_i$  and  $\varepsilon_i$  in proportional histories, e.g.: the constant ratio model [1], Hoffmann-Seeger's model ([10], and Dowling's model [11]. To present these three models, it is necessary to define a few variables involved in their formulation:

- $\tilde{\sigma}_1, \tilde{\sigma}_2, \tilde{\sigma}_3, \tilde{\varepsilon}_1, \tilde{\varepsilon}_2, \tilde{\varepsilon}_3$ : hookean principal stresses and strains at the notch root (elastically calculated using Hooke's law and elastic  $K_\sigma$  and  $K_\varepsilon$ );
- $\tilde{\sigma}_{Mises}, \tilde{\varepsilon}_{Mises}$ : hookean Mises stress and strain (at the notch root), calculated using the above variables;
- $\sigma_1, \sigma_2, \sigma_3, \varepsilon_1, \varepsilon_2, \varepsilon_3$ : elastic-plastic principal stresses and strains (notch root);
- $\sigma_{Mises}, \varepsilon_{Mises}$ : Mises stress and strain (notch root);
- $\lambda_2, \lambda_3$ : ratios between pairs of principal stresses, where  $\lambda_2 = \sigma_2/\sigma_1$  and  $\lambda_3 = \sigma_3/\sigma_1$ , both between -1 and 1;
- $\varphi_2, \varphi_3$ : ratios between pairs of principal strains, where  $\varphi_2 = \varepsilon_2/\varepsilon_1$ ,  $\varphi_3 = \varepsilon_3/\varepsilon_1$ , both between -1 and 1; and
- $\lambda_{Mises}, \varphi_{Mises}$ : Mises ratios  $\lambda_{Mises} = \sigma_{Mises}/\sigma_1$  and  $\varphi_{Mises} = \varepsilon_{Mises}/\varepsilon_1$ .

From the above definitions, it is possible to obtain

$$\lambda_{Mises} = \frac{\sigma_{Mises}}{\sigma_1} = \frac{1}{\sqrt{2}} \sqrt{(1 - \lambda_2)^2 + (1 - \lambda_3)^2 + (\lambda_2 - \lambda_3)^2} \quad (20)$$

$$\phi_{Mises} = \frac{\varepsilon_{Mises}}{\varepsilon_1} = \frac{1}{\sqrt{2}(1 + \nu)} \sqrt{(1 - \phi_2)^2 + (1 - \phi_3)^2 + (\phi_2 - \phi_3)^2} \quad (21)$$

The three models are described next.

### 5.1 Constant ratio model

The *constant ratio model* [1] assumes that, under a proportional history, the bi-axial ratios  $\lambda_2, \lambda_3, \varphi_2$  and  $\varphi_3$  remain constant even after yielding has occurred. Since the elastic Poisson coefficient  $\nu_{el}$  is typically between 1/4 and 1/3 in most metal alloys, significantly different than the plastic  $\nu_{pl} = 0.5$ , these ratios are in fact not constant, but for small plastic strains this is a good approximation.

Thus, these ratios can be estimated from the elastic (hookean) stresses and strains, obtained from Hooke's law using elastic  $K_\sigma$  and  $K_\varepsilon$ :

$$\lambda_2 \cong \frac{\tilde{\sigma}_2}{\tilde{\sigma}_1}, \lambda_3 \cong \frac{\tilde{\sigma}_3}{\tilde{\sigma}_1}, \phi_2 \cong \frac{\tilde{\varepsilon}_2}{\tilde{\varepsilon}_1}, \phi_3 \cong \frac{\tilde{\varepsilon}_3}{\tilde{\varepsilon}_1} \quad (22)$$

Therefore,  $\lambda_{Mises}$  is also a constant, leading to

$$\lambda_{Mises} \cong \frac{\tilde{\sigma}_{Mises}}{\tilde{\sigma}_1} \Rightarrow \tilde{\sigma}_{Mises} \cong \frac{\tilde{\sigma}_1}{\sqrt{2}} \sqrt{(1 - \lambda_2)^2 + (1 - \lambda_3)^2 + (\lambda_2 - \lambda_3)^2} \quad (23)$$

and, similarly,  $\varphi_{Mises}$  can be calculated from  $\varphi_2$  and  $\varphi_3$ . The cyclic  $\sigma$ - $\varepsilon$  relation is then defined using Mises and the Ramberg-Osgood uniaxial parameters

$$\varepsilon_{Mises} = \frac{\sigma_{Mises}}{E} + \left( \frac{\sigma_{Mises}}{H_c} \right)^{1/h_c} \quad (24)$$

297 If no notches are present, then the above equation is used together with the estimates for  $\lambda_{Mises}$ ,  
 298  $\varphi_{Mises}$ ,  $\lambda_2$ ,  $\lambda_3$ ,  $\varphi_2$  and  $\varphi_3$  to obtain  $\sigma_i$  from  $\varepsilon_i$  ( $i = 1, 2, 3$ ), or vice-versa. In notched components,  
 299  $\tilde{\sigma}_{Mises}$  (elastically calculated including the  $K_t$ s) is applied to a variation of the Neuber's rule to  
 300 calculate the Mises elastic-plastic stress  $\sigma_{Mises}$  and, finally,  $\varepsilon_{Mises}$ ,  $\sigma_i$  and  $\varepsilon_i$  ( $i = 1, 2, 3$ ):

$$\frac{(\tilde{\sigma}_{Mises})^2}{E} = \sigma_{Mises} \cdot \varepsilon_{Mises} = \frac{(\sigma_{Mises})^2}{E} + \sigma_{Mises} \cdot \left( \frac{\sigma_{Mises}}{H_c} \right)^{1/h_c} \quad (25)$$

301 After calculating  $\sigma_{Mises}$  and  $\varepsilon_{Mises}$ , the constant ratio model obtains the principal stress and strain  
 302 using:

$$\begin{cases} \sigma_1 = \sigma_{Mises}/\lambda_{Mises}, \sigma_2 = \lambda_2\sigma_1, \sigma_3 = \lambda_3\sigma_1 \\ \varepsilon_1 = \varepsilon_{Mises}/\phi_{Mises}, \varepsilon_2 = \phi_2\varepsilon_1, \varepsilon_3 = \phi_3\varepsilon_1 \end{cases} \quad (26)$$

### 303 5.2 Hoffmann-Seeger's model

304 Hoffmann-Seeger's model [10] uses the same cyclic  $\sigma$ - $\varepsilon$  relation and the same variation of Neuber's  
 305 rule presented above to calculate  $\sigma_{Mises}$  and  $\varepsilon_{Mises}$ , but it assumes that:

- 306 • the critical point happens at the surface, with principal stresses  $\sigma_1$  and  $\sigma_2$ ;
- 307 •  $\sigma_3$  is defined normal to the surface, therefore  $\sigma_3 = 0$  (and then  $\lambda_3 = 0$ ); and
- 308 • only the ratio  $\phi_2 = \tilde{\varepsilon}_2/\tilde{\varepsilon}_1$  is estimated using the linear elastic (hookean) values.

309 After calculating  $\sigma_{Mises}$  and  $\varepsilon_{Mises}$ ,  $\sigma_i$  and  $\varepsilon_i$  are estimated from:

$$\begin{cases} \sigma_1 = \sigma_{Mises}/\bar{\lambda}_{Mises}, \sigma_2 = \bar{\lambda}_2\sigma_1, \sigma_3 = 0 \\ \varepsilon_1 = \frac{(1-\bar{\lambda}_2\bar{\nu})\varepsilon_{Mises}}{\bar{\lambda}_{Mises}}, \varepsilon_2 = \phi_2\varepsilon_1, \varepsilon_3 = -\bar{\nu}\varepsilon_1 \frac{1+\bar{\lambda}_2}{1-\bar{\lambda}_2\bar{\nu}} \end{cases} \quad (27)$$

310

$$\bar{\nu} = \frac{1}{2} - \frac{(1/2 - \nu_{el})\sigma_{Mises}}{E \cdot \varepsilon_{Mises}}, \bar{\lambda}_2 = \frac{\phi_2 + \bar{\nu}}{1 + \phi_2\bar{\nu}}, \bar{\lambda}_{Mises} = \sqrt{1 - \bar{\lambda}_2 + \bar{\lambda}_2^2} \quad (28)$$

### 311 5.3 Dowling's model

312 The model proposed in [11] also assumes that the principal stresses  $\sigma_1$  and  $\sigma_2$  act on the surface of  
 313 the critical point (therefore  $\sigma_3$  is zero), and it considers  $\lambda_2$  and  $\varphi_2$  constant, estimating them from  
 314 their hookean values

$$\lambda_2 = \frac{\sigma_2}{\sigma_1} \cong \frac{\tilde{\sigma}_2}{\tilde{\sigma}_1} \cong \frac{\phi_2 + \nu}{1 + \phi_2\nu}, \phi_2 = \frac{\varepsilon_2}{\varepsilon_1} \cong \frac{\tilde{\varepsilon}_2}{\tilde{\varepsilon}_1} \cong \frac{\lambda_2 - \nu}{1 - \lambda_2\nu} \quad (29)$$

315 Exceptionally,  $\sigma_2$  is defined here as the lowest principal stress at the surface, even if  $\sigma_2$  is smaller  
 316 than  $\sigma_3$  (i.e. the convention  $\sigma_3 \leq \sigma_2 \leq \sigma_1$  is violated if  $\lambda_2 < 0$ ).

317 The greatest difference between the previous two models and Dowling's is that the latter correlates  
 318  $\sigma_1$  and  $\varepsilon_1$  directly using effective Ramberg-Osgood parameters  $E^*$  and  $H_c^*$

$$E^* = \left( \frac{1 + \phi_2 \nu}{1 - \nu^2} \right) \cdot E, \quad H_c^* = H_c \cdot \left( \frac{2}{2 - \lambda_2} \right)^{h_c} (1 - \lambda_2 + \lambda_2^2)^{0.5(h_c - 1)} \quad (30)$$

319 and the effective relation between  $\sigma_1$  and  $\varepsilon_1$  is [11]

$$\varepsilon_1 = \frac{\sigma_1}{E^*} + \left( \frac{\sigma_1}{H_c^*} \right)^{1/h_c} \quad (31)$$

320 Figure 7 presents the principal stress-strain relation for the 1020 steel, according to Dowling's model.

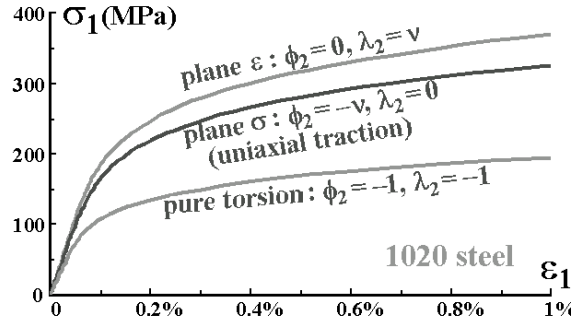


Figure 7: Principal stress-strain relations under plane strain, plane stress and pure torsion, according to Dowling.

321 In notched components, another variation of Neuber's rule must be used to calculate  $\sigma_1$  (and then  
 322  $\varepsilon_1$ ) from  $\tilde{\sigma}_{Mises}$ :

$$\frac{(\tilde{\sigma}_{Mises})^2}{E} = \sigma_1 \cdot \varepsilon_1 = \frac{\sigma_1^2}{E^*} + \sigma_1 \cdot \left( \frac{\sigma_1}{H_c^*} \right)^{1/h_c} \quad (32)$$

323 The other principal stresses and strains are obtained from  $\sigma_1$  and  $\varepsilon_1$ :

$$\begin{aligned} \sigma_2 &= \lambda_2 \sigma_1, \quad \sigma_3 = 0 \\ \varepsilon_2 &= \phi_2 \varepsilon_1, \quad \varepsilon_3 = -\bar{\nu} \varepsilon_1 \frac{1 + \lambda_2}{1 - \lambda_2 \bar{\nu}}, \quad \bar{\nu} = \frac{1}{2} - \left( \frac{1}{2} - \nu \right) \frac{\sigma_1}{E^* \varepsilon_1} \end{aligned} \quad (33)$$

324 The largest shear strain  $\gamma_{max}$  can then be calculated from the maximum difference between the  
 325 principal strains  $\varepsilon_i$  ( $i = 1, 2, 3$ ), obtaining not only its magnitude but also the plane where this  
 326 maximum occurs.

327 It is important to note that the three presented models (formulated using the cyclic  $\sigma$ - $\varepsilon$  curve) can  
 328 also be applied to the hysteresis loops equations, by replacing in each equation  $\varepsilon$  with  $\Delta\varepsilon/2$  and also  
 329  $\sigma$  with  $\Delta\sigma/2$ . The presented models are compared next.

### 330 6 Comparison among the multiaxial models

331 The presented multiaxial models are compared considering a notched 1020 steel shaft with diameter  
 332  $d$  equal to 60mm under alternate bending moment  $M_a$  of 2kNm and torsion  $T_a$  of 3kNm, in phase,  
 333 with stress concentration factors in bending  $K_{tM}$  equal to 3.4 and in torsion  $K_{tT}$  equal to 2.4.

334 Assuming the alternate nominal stress  $\sigma_{na}$  as elastic,

$$\sigma_{na} = \frac{\sqrt{(32M_a)^2 + 3(16T_a)^2}}{\pi d^3} \quad (34)$$

335 then  $\sigma_{na} = 155\text{MPa}$ . This stress is lower than the cyclic yielding strength  $S_{yc} = 241\text{MPa}$ , therefore  
 336 the hypothesis of  $\sigma_{na}$  elastic is valid.

337 Using the “highest  $K_t$  method” through the highest  $K_t = 3.4$ ,  $\sigma_a$  and  $\varepsilon_a$  are calculated using Mises  
 338 and Neuber

$$(K_t \sigma_{na})^2 = (3.4 \cdot 155)^2 = \sigma_a \varepsilon_a E = \sigma_a^2 + 203000 \cdot \sigma_a \left(\frac{\sigma_a}{772}\right)^{1/0.18} \Rightarrow \begin{cases} \sigma_a = 279\text{MPa} \\ \varepsilon_a = 0.49\% \end{cases} \quad (35)$$

339 and then the life  $N$  estimated for the shaft is

$$\frac{\Delta\varepsilon}{2} = \varepsilon_a = \frac{896}{203000} (2N)^{-0.12} + 0.41(2N)^{-0.51} \Rightarrow N = 5871 \text{ cycles} \quad (36)$$

340 To use the multiaxial stress-strain models, the hookean stresses at the notch root are calculated  
 341 considering  $K_{tM} = 3.4$  and  $K_{tT} = 2.4$  as purely elastic:

$$\tilde{\sigma}_{a_{Mises}} = \sqrt{(K_{tM}\sigma_M)^2 + 3(K_{tT}\tau_T)^2} = \frac{\sqrt{(3.4 \cdot 32 \cdot M_a)^2 + 3(2.4 \cdot 16 \cdot T_a)^2}}{\pi(0.060)^3} \quad (37)$$

342

$$\tilde{\sigma}_{a_{1,2}} = \frac{K_{tM}\sigma_M}{2} \pm \sqrt{\left(\frac{K_{tM}\sigma_M}{2}\right)^2 + (K_{tT}\tau_T)^2} = 160 \pm 234\text{MPa} \quad (38)$$

343 Thus, the hookean stresses are  $\tilde{\sigma}_{a_{Mises}} = 435\text{MPa}$ ,  $\tilde{\sigma}_{a_1} = 394\text{MPa}$ ,  $\tilde{\sigma}_{a_2} = -73\text{MPa}$  and  $\tilde{\sigma}_{a_3} = 0$ ,  
 344 which can be correlated to the principal hookean strains from Hooke's law (considering  $\nu = 0.3$ ):

$$\begin{aligned}
\tilde{\varepsilon}_{a_1} &= [394 - 0.3(-73 + 0)]/203000 = 0.205\% \\
\tilde{\varepsilon}_{a_2} &= [-73 - 0.3(394 + 0)]/203000 = -0.094\% \\
\tilde{\varepsilon}_{a_3} &= [0 - 0.3(-73 + 394)]/203000 = -0.047\%
\end{aligned} \tag{39}$$

345

$$\tilde{\varepsilon}_{a_{Mises}} = \frac{1}{\sqrt{2}(1 + \nu)} \sqrt{(\tilde{\varepsilon}_{a_1} - \tilde{\varepsilon}_{a_2})^2 + (\tilde{\varepsilon}_{a_1} - \tilde{\varepsilon}_{a_3})^2 + (\tilde{\varepsilon}_{a_2} - \tilde{\varepsilon}_{a_3})^2} = 0.214\% \tag{40}$$

346

From the constant ratio and Hoffmann-Seeger models,

$$\frac{\tilde{\sigma}_{a_{Mises}}^2}{E} = 0.93 = \frac{\sigma_{a_{Mises}}^2}{E} + \sigma_{a_{Mises}} \cdot \left( \frac{\sigma_{a_{Mises}}}{772} \right)^{1/0.18} \Rightarrow \sigma_{a_{Mises}} = 259 \text{ MPa} \tag{41}$$

347

$$\varepsilon_{a_{Mises}} = \frac{\sigma_{a_{Mises}}}{203000} + \left( \frac{\sigma_{a_{Mises}}}{772} \right)^{1/0.18} \Rightarrow \varepsilon_{a_{Mises}} = 0.360\% \tag{42}$$

348

Note, as expected, that  $\sigma_{a_{Mises}} < \tilde{\sigma}_{a_{Mises}}$  and  $\varepsilon_{a_{Mises}} > \tilde{\varepsilon}_{a_{Mises}}$ .

349

350

351

From the constant ratio model, the hookean stresses and strains can be used to estimate  $\lambda_{Mises} = 1.105$ ,  $\lambda_2 = -0.185$ ,  $\lambda_3 = 0$ ,  $\varphi_{Mises} = 1.046$ ,  $\varphi_2 = -0.460$  and  $\varphi_3 = -0.231$ , so the alternate principal stresses and strains are

$$\begin{aligned}
\sigma_{a_1} &= 259/1.1 = 235 \text{ MPa}, \quad \sigma_{a_2} = \lambda_2 \sigma_{a_1} = -44 \text{ MPa}, \quad \sigma_{a_3} = 0 \\
\varepsilon_{a_1} &= 0.359\%/1.046 = 0.344\%, \quad \varepsilon_{a_2} = \phi_2 \varepsilon_{a_1} = -0.158\%, \quad \varepsilon_{a_3} = \phi_3 \varepsilon_{a_1} = -0.080\%
\end{aligned} \tag{43}$$

352

On the other hand, Hoffmann-Seeger's model predicts

$$\begin{aligned}
\bar{\nu} &= \frac{1}{2} - \left( \frac{1}{2} - \nu \right) \frac{\sigma_{a_{Mises}}}{E \cdot \varepsilon_{a_{Mises}}} = 0.5 - 0.2 \frac{259}{203000 \cdot 0.00359} = 0.429 \\
\bar{\lambda}_2 &= \frac{\phi_2 + \bar{\nu}}{1 + \phi_2 \bar{\nu}} = \frac{-0.46 + \bar{\nu}}{1 - 0.46 \bar{\nu}} = -0.0387, \quad \bar{\lambda}_{Mises} = \sqrt{1 - \bar{\lambda}_2 + \bar{\lambda}_2^2} = 1.02
\end{aligned} \tag{44}$$

353

resulting in alternate principal stresses and strains

$$\begin{cases} \sigma_{a_1} = 259/1.02 = 254 \text{ MPa}, \quad \sigma_{a_2} = -0.0387 \cdot \sigma_{a_1} = -10 \text{ MPa}, \quad \sigma_{a_3} = 0 \\ \varepsilon_{a_1} = (1 - \bar{\lambda}_2 \bar{\nu}) 0.360\%/1.02 = 0.359\%, \quad \varepsilon_{a_2} = \phi_2 \varepsilon_{a_1} = -0.165\% \\ \varepsilon_{a_3} = -\bar{\nu} \varepsilon_{a_1} (1 + \bar{\lambda}_2) / (1 - \bar{\lambda}_2 \bar{\nu}) = -0.146\% \end{cases} \tag{45}$$

354

355

Dowling's model uses the elastic ratios  $\lambda_2 = -0.185$  and  $\varphi_2 = -0.460$  to calculate the effective parameters of the hardening curve

$$E^* = \left( \frac{1 + \phi_2 \nu}{1 - \nu^2} \right) \cdot E = \left( \frac{1 - 0.46 \cdot 0.3}{1 - 0.3^2} \right) \cdot 203 \text{GPa} = 192 \text{GPa} \quad (46)$$

$$H_c^* = 772 \text{MPa} \cdot \left( \frac{2}{2 - \lambda_2} \right)^{0.18} (1 - \lambda_2 + \lambda_2^2)^{0.5(0.18-1)} = 700 \text{MPa} \quad (47)$$

$$\frac{(\tilde{\sigma}_{a_{Mises}})^2}{E} = 0.93 = \sigma_{a1} \cdot \varepsilon_{a1} = \frac{\sigma_{a1}^2}{E^*} + \sigma_{a1} \cdot \left( \frac{\sigma_{a1}}{H_c^*} \right)^{1/h_c} \Rightarrow \begin{cases} \sigma_{a1} = 240 \text{MPa} \\ \varepsilon_{a1} = 0.388\% \end{cases} \quad (48)$$

$$\begin{cases} \sigma_{a2} = \lambda_2 \sigma_{a1} = -45 \text{MPa}, \sigma_{a3} = 0 \\ \varepsilon_{a2} = \phi_2 \varepsilon_{a1} = -0.179\%, \varepsilon_{a3} = -\bar{\nu} \varepsilon_{a1} \frac{1+\lambda_2}{1-\lambda_2 \bar{\nu}} = -0.127\% (\bar{\nu} = 0.436) \end{cases} \quad (49)$$

For all considered models, the maximum shear strain amplitude is calculated from  $\gamma_{amax} = \varepsilon_{a1} - \varepsilon_{a2}$ , assuming that the directions 1 and 2 are respectively the ones with maximum and minimum principal strains. The maximum normal strains and stresses in the plane of  $\gamma_{amax}$  are

$$\varepsilon_{a\perp} = (\varepsilon_{a1} + \varepsilon_{a2})/2 \quad \text{and} \quad \sigma_{a\perp} = (\sigma_{a1} + \sigma_{a2})/2 \quad (50)$$

Since in this problem the mean stresses and strains are zero, the values used by the Brown-Miller, Fatemi-Socie and SWT strain-life models are respectively  $\Delta\varepsilon_{\perp} = 2\varepsilon_{a\perp}$ ,  $\sigma_{\perp max} = \sigma_{a\perp}$  and  $\sigma_{\perp 1max} = \sigma_{a1}$ .

Table 1 summarizes the stresses and strains obtained from the hookean values (obtained assuming elastic stresses, which must not be used in life predictions in the presence of significant plasticity), from the “highest  $K_t$  method”, and from the three presented multiaxial stress-strain models: the constant ratio, Hoffmann-Seeger’s and Dowling’s.

Note from Table 1 that the “highest  $K_t$  method” is conservative, especially for the calculated strains, but not too much, therefore it could be used in practice. The three multiaxial models are in theory more accurate, predicting approximately the same values.

Now, using e.g. Dowling’s model, the fatigue life  $N$  can be obtained from the several damage models. Considering the  $\varepsilon N$  curve and using the Mises strain  $\varepsilon_{a_{Mises}} = 0.418\%$ , then it is found that  $N = 8765$  cycles.

If, instead of the  $\varepsilon N$  curve, the  $\gamma N$  curve is considered, estimating its coefficients from  $\tau_c \cong \sigma_c / \sqrt{3}$ ,  $b_{\gamma} \cong b$ ,  $\gamma_c \cong \varepsilon_c \sqrt{3}$  and  $c_{\gamma} \cong c$ , and using  $\gamma_{amax} = 0.567\%$ , then it is found that  $N = 14693$  cycles.

Considering the Brown-Miller’s model, with its constants estimated from  $\alpha_{BM} \cong 0.3$ ,  $\beta_1 = 1.3 + 0.7 \cdot \alpha_{BM} = 1.51$  and  $\beta_2 = 1.5 + 0.5 \cdot \alpha_{BM} = 1.65$ , with  $\Delta\varepsilon_{\perp} = 0.209\%$ , then it is found that  $N = 10290$  cycles.

Fatemi-Socie’s model, using  $\alpha_{FS} \cong S_{yc} / \sigma_c = 241 \text{MPa} / 896 \text{MPa} \cong 0.27$  and the  $\gamma N$  curve estimated as above, where  $\sigma_{\perp max} = 98 \text{MPa}$ , results in  $N = 11201$  cycles.

And finally, considering the SWT’s model, which is appropriate for materials more sensitive to normal stresses, with  $\Delta\varepsilon_1 / 2 = \varepsilon_{a1} = 0.388\%$  and, since the mean loads are zero,  $\sigma_{\perp 1max} = \sigma_{a1} = 240 \text{MPa}$ , then  $N = 13577$  cycles.

Table 1: Stresses (in MPa) and strains predicted from the studied models.

	hookean values	highest $K_t$ method	constant ratio	Hoffman-Seeger	Dowling
$\sigma_{aMises}$	435	279	259	259	265
$\varepsilon_{aMises}$	0.214%	0.488%	0.360%	0.360%	0.418%
$\sigma_{a_1}$	394	253	235	254	240
$\sigma_{a_2}$	-73	-47	-44	-10	-45
$\sigma_{a_3}$	0	0	0	0	0
$\varepsilon_{a_1}$	0.205%	0.466%	0.344%	0.359%	0.388%
$\varepsilon_{a_2}$	-0.094%	-0.215%	-0.158%	-0.165%	-0.179%
$\varepsilon_{a_3}$	-0.047%	-0.108%	-0.080%	-0.146%	-0.127%
$\gamma_{a_{max}}$	0.299%	0.681%	0.502%	0.524%	0.567%
$\Delta\varepsilon_{\perp}$	0.111%	0.251%	0.186%	0.194%	0.209%
$\sigma_{\perp_{max}}$	160	103	95	122	98

385 The above results, based on stresses and strains from Dowling's model, are recalculated considering  
386 hookean values, the "highest  $K_t$  method", the constant ratio and Hoffmann-Seeger models, using the  
387 ViDa fatigue design software [12, 13]. The results are shown in Table 2.

Table 2: Fatigue lives (in cycles) predicted from the studied multiaxial models.

	Mises + $\varepsilon N$ curve	$\gamma N$ curve	Brown-Miller	Fatemi-Socie	SWT
hookean values	59500	94300	63000	56200	18300
highest $K_t$ method	5900	9120	6440	6940	8470
constant ratio	13000	20300	14100	15500	18300
Hoffmann-Seeger	13000	18100	12600	12900	14200
Dowling	8770	14700	10300	11200	13600

388 Except from the results obtained from the hookean values (which are significantly non-conservative),  
389 all combinations of multiaxial damage models with multiaxial stress-strain relations resulted in pre-  
390 dicted lives not too different, varying between 5900 and 20300 cycles. Therefore, it is reasonable to  
391 consider in proportional histories the use of simplifications such as the "highest  $K_t$  method" and the  
392  $\varepsilon N$  curve applied to  $\Delta\varepsilon_{Mises}/2$ , despite the conservative predictions.

393 The hookean values result in poor estimates, overestimating  $\sigma_{a_1}$  and underestimating  $\varepsilon_{a_1}$ , but it  
394 interestingly estimates quite well the product  $\sigma_{a_1}\varepsilon_{a_1}$  (because, according to Neuber,  $\tilde{\sigma}_{a_1}\tilde{\varepsilon}_{a_1} \cong \sigma_{a_1}\varepsilon_{a_1}$ ),  
395 therefore they resulted in good predictions when combined with SWT's model, which is based on this  
396 product.

397 But in NP histories, the NP hardening can have a significant effect in the fatigue life. In addition,  
398 none of the presented  $\sigma$ - $\varepsilon$  models is valid in the NP case (because all of them assumed  $\varphi_2$  constant).  
399 In the NP case, incremental plasticity models must be used [1].

## 400 7 Conclusions

401 In this work, the multiaxial damage models of Sines, Findley and Dang Van, applicable to long fatigue  
402 lives, and Brown-Miller, Fatemi-Socie and Smith-Watson-Topper (SWT), which consider plasticity,  
403 were reviewed. The Sines model is easy to compute, it considers the effect of the second principal  
404 stress  $\sigma_2$  (because it uses the Mises plane), but it is only valid for proportional histories. On the other  
405 hand, Findley's model is hard to compute, because it requires the search for a critical plane, but for  
406 long lives it is valid for any load history, proportional or NP. Dang Van's model is able to consider  
407 the damage in a mesoscopic scale, but it has the limitations of the stress-based models.

408 The strain-based models are valid for any life, short or long. Among them, the Brown-Miller and  
409 Fatemi-Socie models give more value to the shear strains  $\gamma$ , while SWT does it for normal strains  
410  $\varepsilon$ . Brown-Miller and Fatemi-Socie combine  $\Delta\gamma_{max}$  to  $\Delta\varepsilon_{\perp}$  or to  $\sigma_{\perp max}$  normal to the direction of  
411  $\gamma_{max}$ , being applicable to proportional or NP histories. SWT uses the principal strain  $\varepsilon_1$ . The most  
412 versatile models among the studied ones are the Fatemi-Socie and SWT, because they can include the  
413 NP hardening effect. But in order to generate a more realistic model, it is important to modify these  
414 criteria to calculate the fatigue life in the critical plane where the damage parameters of each model  
415 are maximized.

416 The main multiaxial stress-strain models were also reviewed and compared. It can be concluded  
417 that multiaxial stress-strain relations must be used instead of uniaxial ones, even though a few sim-  
418 plifications are adequate, such as the "highest  $K_t$  method" for notched components. Since the critical  
419 point of a structure is usually in its surface, in general a 2D analysis (under plane stress) is enough  
420 for multiaxial fatigue design. Except for the results from the hookean values, which are significantly  
421 non-conservative, all combinations of strain-based multiaxial damage models with multiaxial stress-  
422 strain relations resulted in not too different lives (within a factor of 2) for the considered example,  
423 which has significant plastic strains (but they were not much higher than the elastic ones). The best  
424 predictions should be the ones from multiaxial models that use the critical plane idea, where the  
425 damage parameters are maximized. However, none of the studied stress-strain models is valid for NP  
426 hardening, which can have a significant influence in the fatigue lives of e.g. stainless steels.

## 427 References

428 [1] Socie, D.F. & Marquis, G.B., Multiaxial fatigue. *SAE International*, 1999.

- 429 [2] Zouain, N., Mamiya, E.N. & Comes, F., Using enclosing ellipsoids in multiaxial fatigue strength  
430 criteria. *European Journal of Mechanics - A, Solids*, **25**, pp. 51–71, 2006.
- 431 [3] Sines, G., Behavior of metals under complex static and alternating stresses. *Metal Fatigue*,  
432 McGraw-Hill, pp. 145–169, 1959.
- 433 [4] Findley, W.N., A theory for the effect of mean stress on fatigue of metals under combined torsion  
434 and axial load or bending. *Journal of Engineering for Industry*, pp. 301–306, 1959.
- 435 [5] Dang Van, K. & Papadopoulos, I.V., *High-Cycle Metal Fatigue*. Springer, 1999.
- 436 [6] Gonçalves, C.A., Araújo, J.A. & Mamiya, E.N., Multiaxial fatigue: a stress based criterion for  
437 hard metals. *International Journal of Fatigue*, **27**, pp. 177–187, 2005.
- 438 [7] Brown, M. & Miller, K.J., A theory for fatigue under multiaxial stress-strain conditions. *Institute*  
439 *of Mech Engineers*, **187**, pp. 745–756, 1973.
- 440 [8] Fatemi, A. & Socie, D.F., A critical plane approach to multiaxial damage including out-of-phase  
441 loading. *Fatigue and Fracture of Eng Materials and Structures*, **11(3)**, pp. 149–166, 1988.
- 442 [9] Smith, R.N., Watson, P. & Topper, T.H., A stress-strain parameter for the fatigue of metals. *J*  
443 *of Materials*, **5(4)**, pp. 767–778, 1970.
- 444 [10] Hoffmann, M. & Seeger, T., A generalized method for estimating multiaxial elastic-plastic notch  
445 stresses and strains, Part 1: Theory. *J Eng Materials & Technology*, **107**, pp. 250–254, 1985.
- 446 [11] Dowling, N.E., Brose, W.R. & Wilson, W.K., Notched member fatigue life predictions by the  
447 local strain approach. *Fatigue Under Complex Loading: Analysis and Experiments, AE-6, SAE*,  
448 1977.
- 449 [12] Meggiolaro, M.A. & Castro, J.T.P., Vida 98 - danômetro visual para automatizar o projeto à  
450 fadiga sob carregamentos complexos. *Journal of the Brazilian Society of Mechanical Sciences*,  
451 **20(4)**, pp. 666–685, 1998.
- 452 [13] Miranda, A.C.O., Meggiolaro, M.A., Castro, J.T.P., Martha, L.F. & Bittencourt, T.N., Fatigue life  
453 and crack path prediction in generic 2D structural components. *Engineering Fracture Mechanics*,  
454 **70**, pp. 1259–1279, 2003.